Chapter 7
Print ISBN: 978-93-49238-13-8, eBook ISBN: 978-93-49238-65-7

Dynamic and Physical Processes Associated with Orographic Precipitation in a Conditionally Unstable, Low-cape and High-speed Wind

Gökhan Sever [a] and Yuh-Lang Lin [b*]

DOI: https://doi.org/10.9734/bpi/geserh/v4/4126

Peer-Review History:
This chapter was reviewed by following the Advanced Open Peer Review policy. This chapter was thoroughly checked to prevent plagiarism. As per editorial policy, a minimum of two peer-reviewers reviewed the manuscript. After review and revision of the manuscript, the Book Editor approved the manuscript for final publication. Peer review comments, comments of the editor(s), etc. are available here: https://peerreviewarchive.com/review-history/4126

ABSTRACT

Orographic effects on precipitation in a conditionally unstable, low convective available potential energy (CAPE), and high-speed wind are investigated by a series of systematic two- and three-dimensional idealized numerical experiments. Sensitivity experiments are performed with a flow with low CAPE to assess the evolution of orographic precipitation in an environment similar to that observed in tropical cyclones, which, unexpectedly, show that precipitation is nearly doubled compared to that with high CAPE. The heavy rain production in the low CAPE case is explained by the following microphysical processes: (1) warm-rain formation processes (auto-conversion and accretion) are more effective, and (2) strong downdraft and advection-induced evaporation tend to deplete precipitation before reaching the ground, which overcomes the intense rain production via graupel and snow melting in high CAPE case. Overall, both in 2D and 3D high-wind simulations, the pattern of the precipitation distribution resembles the bell-shaped mountain profile with the maximum located over the mountain peak, which may be applicable to climate prediction of orographic precipitation.

Keywords: Dynamic; physical processes; orographic precipitation; high-speed wind.

1. INTRODUCTION

Under the orographically modified upstream airflow associated with the large-scale environment, the interaction between the dynamic processes and cloud

[a] Argonne National Laboratory, Lemont, Illinois, USA.
[b] North Carolina A&T State University, Greensboro, North Carolina, USA.
**Corresponding author: E-mail: ylin@ncat.edu.*

microphysical processes (Sawyer 1956) is extremely complicated, which makes quantitative forecasting of orographic precipitation extremely difficult (e.g., see Lin 2007 for a detailed review). In particular, when tropical cyclones pass over a mesoscale mountain, such as the Appalachian Mountains in the U. S. (e.g., Hurricane Ivan (2004)), the Hispaniola and Puerto Rico Mountains of the Caribbean Sea (e.g., Hurricanes Jeanne (2004) and Maria (2017)), La Reunion and Madagascar islands of the Indian Ocean (e.g., Tropical Cyclone Gamede (2007)), Central Mountain Ranges (CMR) of Taiwan (e.g., Typhoon Morakot (2009), they all resulted in heavy rainfall accumulations (Chow et al. 2012). Although isolated islands have been subject to many orographic precipitation studies, robust quantitative precipitation forecast (QPF) remains one of the most challenging problems in numerical weather prediction. The devastating results of extreme precipitation events associated with orography, which include property damage and loss of lives, demand more studies on an orographic precipitation phenomenon in order to improve our preparedness.

In order to understand the basic dynamics of orographic rain, Chu and Lin (2000) studied the effects of orography, gravity waves, and density currents on the propagation and generation of convective systems in a conditionally unstable airflow over an idealized mesoscale mountain using a two-dimensional model. Based on idealized simulations of conditionally unstable flow over a bell-shaped mountain using the Advanced Regional Prediction System (ARPS) model, they identified three moist flow regimes: 1) an upstream propagating system, 2) a quasi-stationary convective system, and 3) quasi-stationary and downstream propagating systems. In regime 1, the generation of convective cells was attributed to upstream deceleration associated with orographic forcing, gravity waves at earlier stages, and density current at later stages. The heavy rainfall was produced over the upslope and propagated downstream once the density current developed. In regime 2, the convective system transitioned to quasi-stationary over the mountain peak. Orographic forcing and gravity waves are the main forces that drove convective cells in this regime. In regime 3, a quasi-stationary and a downstream propagating mode were identified. The quasi-stationary system formed on the same basis as in regime 2. However, the convergence associated with a hydraulic jump over the lee slope was attributed to the formation of downstream propagating convective cells. Evaporative cooling was noted as an important process for the triggering of new cells far upstream of the mountain.

Chu and Lin's (2000) study was extended by Chen and Lin (2005) to include the effects of convective available potential energy (CAPE) and unsaturated moist Froude number (F_w) and for a conditionally unstable flow over a two-dimensional idealized mountain were investigated to further study the propagation and types and of orographic cloud precipitation systems using the Weather Research and Forecast (WRF) model and the Schlesinger's (1978) conditionally unstable sounding. They developed a moist flow regime diagram, based on the F_w and CAPE parameters. Regime 1 is characterized by a convective system propagating in the upstream direction and a slow-moving convective system over the mountaintop. Regime 2 is characterized by long-lasting by a convective

system over the upslope and mountain summit. Regime 3 has characteristics of a convective/mixed/stratiform orographic precipitation system over the barrier, and a downwind propagating convective system. A new regime was also identified, which is regime 4. This regime has characteristics of an orographic stratiform system over the mountain and a downstream propagating convective system. Similar to Chu and Lin (2000) study, the convective system propagation was explained by the orographic blocking and density current formed by evaporative cooling to suppress the basic flow.

In order to apply Chu and Lin's (2000) moist flow regimes to the orographic rain dynamics, Sever and Lin (2017) extend the flow speed of [2.5, 15 ms^{-1}] to greater than 36 m s^{-1}. They conducted a series of systematic two- and three-dimensional (2D and 3D) idealized numerical experiments to investigate the combined effects of dynamical and physical processes on orographic precipitation with varying incoming basic flow speed (U) in a conditionally unstable uniform flow of CAPE = 1900 J kg^{-1}. In addition to the three moist flow regimes found in Chu and Lin at lower wind speeds, a new flow regime, Regime IV, is found for higher wind speeds (U > 36 m s^{-1}) and is characterized by gravity waves and heavy precipitation and lack of upper-level wave breaking and turbulence over the lee slope. The regime transition from III to IV at 36 m s^{-1} is explained by the transition from upward propagating gravity waves to evanescent flow, which can be predicted with a modified mountain wave theory. Although the basic features are captured well in low grid resolution (Δx = 1 km), high resolution (Δx = 100 m) 2D and 3D simulations are required to resolve precipitation distribution and intensity at higher basic winds (U > 30 m s^{-1}). Based on 3D simulations, gravity wave-induced severe downslope winds and turbulent mixing within the hydraulic jump reduce orographic precipitation in Regime III. A preliminary budget analysis indicated that, in Regime IV, orographic precipitation further increases due to enhanced rain processes when the blocking effect of wave breaking vanishes.

In a more relevant paper, Yang et al. (2011) analyzed Typhoon Nari (2001) from vapor, cloud and precipitation budget perspective in order to improve the understanding of the typhoon's cloud and precipitation processes. The analyses are conducted on relatively high spatial-temporal resolution (2-km horizontal grid size and 2-min time interval) outputs from the fifth-generation Mesoscale Model (MM5). Their initial focus is on the budget evolution, particularly while the typhoon is moving from over the ocean to pass over Taiwan's Central Mountain Range (CMR). They conclude that evaporation from the ocean contributes only about 10% of the total inward horizontal vapor transport over the ocean. Only about 5% of ocean-originated water vapor is encountered in the inner core regions.

In this study, the sensitivity analyses include variations of CAPE as well as the basic wind speed (U). This extends the conditionally unstable moist flow and orographic precipitation studies into a 2D parameter space. A broader parameter space of CAPE (i.e., from 2000 to 100 J kg^{-1}) and U (i.e., from 1 to 50 m s^{-1}) spans a large parameter space and thus many hundreds of simulations (assuming both parameters will be incremented more finely). Thus, we first

considered the evolution of the precipitating system and the impacts of CAPE variation from very low to high CAPE (100 to 2000 J kg^{-1}) and other environmental factors, which will be analyzed in more detail.

Simulations with a high CAPE environment analyzed in the previous studies are more representative of the supercell environment due to the use of the Weisman and Klemp (1982) sounding. In order to investigate the orographic impacts on the precipitation associated with tropical cyclones, i.e., orographic TC-rain, a set of low CAPE experiments is designed. In particular, we are interested in understanding how a system can produce heavy orographic precipitation in a low CAPE environment under high winds, and if so, what are the main dynamical and physical differences in the evolution of this system compared to those simulated with high CAPEs?

Previously, Chen and Lin (2005) hypothesized that, in addition to the unsaturated moist Froude number F_w, CAPE may impact moist flow regimes. The hypothesis was tested by varying the F_w and CAPE for a conditionally unstable environment over an idealized 2D mountain. It was found that under low CAPE conditions, orographic precipitation can be modulated by large horizontal wind speeds. The implication for a tropical cyclone is that the system does not necessarily require high CAPE to produce heavy orographic rainfall. However, the combination of high CAPE and *U* leads to differing precipitation intensities and types. Highly convective precipitation is observed on the upwind side of the mountains for weaker flow, with a transition to stratiform systems over the mountaintop and convective systems moving downward for stronger wind speeds. Based on a conditionally unstable Schlesinger (1978) sounding, they identified four moist flow regimes, Regime I: flow with an upstream propagating convective system; Regime II: flow with a long-lasting orographic convective system; Regime III: mixed convective/stratiform system over the mountain and downstream propagation. Furthermore, a new moist flow regime, which is different than in Chu and Lin (2000), Regime IV, was identified and characterized by Chen and Lin (2005) by a stratiform orographic precipitation system over the mountain and a downstream propagating cloud system. The four moist flow regimes determined by different combinations of F_w and CAPE are shown in Fig. 1.

Huang and Lin (2014) investigate the three-dimensional structural evolution of Typhoon Morakot (2009), and the common factors explaining the extreme heavy rainfall within the vicinity of the Central Mountain Range (CMR) of Taiwan. They particularly focus on the track, deflection of track, rainband features, and precipitation structure of the typhoon based on numerical simulations. They found that extremely heavy rainfall is attributed to strong upward motions caused by orographic lifting in the presence of high water vapor, with a note that instability might have contributed to the heavy rainfall.

Previous studies, such as Chen and Lin (2005) and Miglietta and Rotunno (2010), studied orographic precipitation in a low CAPE environment, yet neither of these studies extended simulations to high wind regimes (i.e., $U > 25$ m s^{-1}). These simulations presented in this section extend to $U = 40$ m s^{-1}. Most notably

high resolution 2D and 3D-LES (Δx = Δy = 0.1 km) distinguish these results from those of Chen and Lin (2005) which focus only on 2D low resolution (Δx = 1 km) simulations.

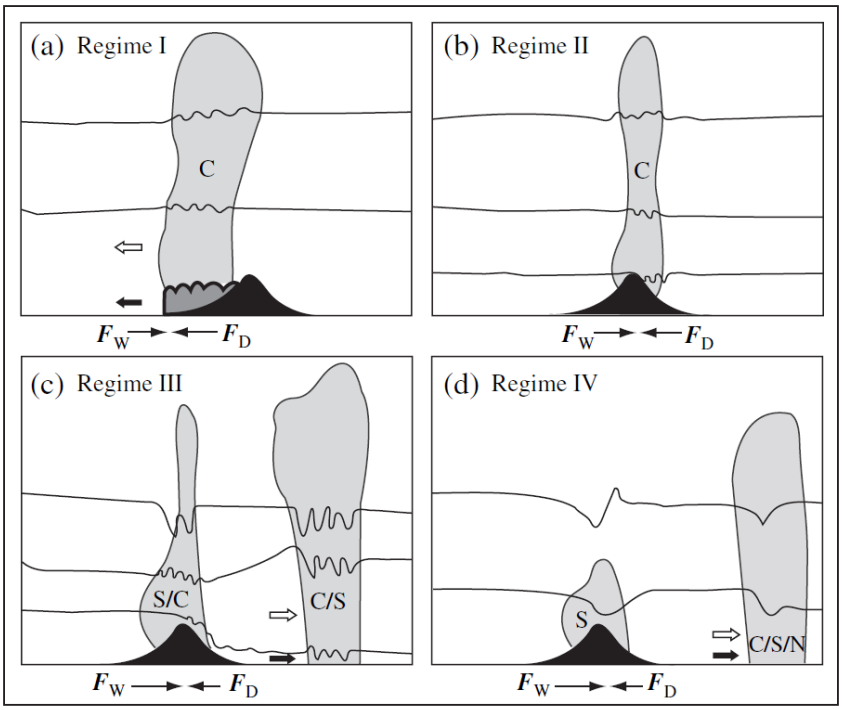

Fig. 1. Schematic of the four moist flow regimes for a conditionally unstable airflow over a mesoscale mountain for (F_w, *CAPE*): (a) (small, large), (b) (small, small), (c) (large, large), and (d) (large, small). Below each panel, F_W and F_D denote the forcing associated with the basic flow and density current/cold pool, respectively. Lines of constant potential temperature (isentropes) and cloud boundaries are denoted by solid lines and gray filled shapes, respectively. Symbols C, S, and N denote convective, stratiform, and no-cloud types, respectively. Outline (filled) arrow denotes the propagation direction of the precipitation system (density current). (Chen and Lin 2005; Lin 2007)

In Section 2, the numerical experimental design is described. The sensitivity of orographic precipitation to resolution and dimensionality will be discussed in Section 3. Evolutions of precipitating systems at higher wind regimes and the formation of heavy precipitation will be investigated in Sections 4 and 5, respectively. The impact of moisture, stability, and wind speed on orographic flow will be studied in Section 6. Concluding remarks can be found in Section 7.

2. NUMERICAL EXPERIMENTAL DESIGN

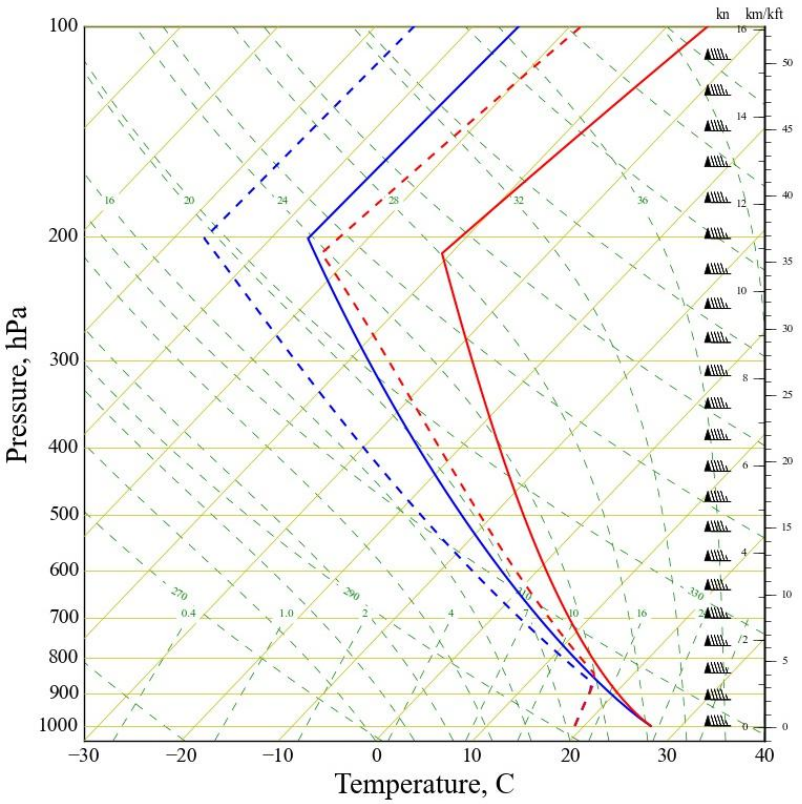

Fig. 2. Skew-T diagram of the idealized soundings used for all CAPE sensitivity simulations. The blue line set is the original CAPE = 2000 J kg^{-1} sounding, whereas the red line set is for low CAPE (=100 J kg^{-1}) cases. (Weisman and Klemp 1982)

A series of idealized 2D low- and high-resolution simulations and 3D LESs are conducted by CM1 (release 17) (Bryan and Fritsch 2002). Topography is the same as that in Sever and Lin (2017). CAPE is varied by increasing the tropopause temperature, similar to Miglietta and Rotunno (2009). In this process, the relative humidity (RH) of the sounding is kept constant, while some other parameters of the sounding have been changed. The LFC of the sounding increased to 722 mb for low CAPE cases (CAPE = 100 J kg^{-1}) from its base state of 829 mb at 2000 J kg^{-1}. The CIN also enhanced from -44 J kg^{-1} to -108 J kg^{-1}. Most noticeably, the upper levels of the atmosphere become warmer because of temperature increases at upper levels. In addition, the vapor mixing ratio is increased in low CAPE cases as the RH is kept constant. There are other ways

to alter the CAPE, such as, by changing the lower-level temperature or moisture profile, by altering the structure of the sounding above LFC, and by keeping the mixing ratio constant instead of RH. However, these changes would complicate the comparison with previous studies; thus, we focused on the current method. Fig. 2 shows the temperature and dew-point profiles of low CAPE (red) and high CAPE (blue) on a Skew T-Log P diagram.

The Goddard LFO microphysics scheme is chosen as before to simulate the precipitation formation. The 1.5-order turbulent kinetic energy (TKE) closure is chosen for the subgrid turbulence scheme. The key physical model assumptions are that free slip boundary conditions are specified at the bottom boundary, and PBL and radiation schemes, as well as the Coriolis effect, are turned off.

3. THE SENSITIVITY OF OROGRAPHIC PRECIPITATION TO RESOLUTION AND DIMENSIONALITY

Before carrying out the flow evolution analysis at high wind speeds, it is first shown how the results are sensitive to the horizontal grid resolution and dimensions. Fig. 3 shows the 12h total rainfall over large and zoomed domains for 2D-Low and 2D-High cases. Precipitation accumulation becomes visible after 5 m s^{-1} in both cases. This can be explained by the higher LFC in the lower CAPE soundings, whereby higher wind speeds are required to trigger the conditional instability embedded in the upcoming flow. With lower wind, the system does not show a sign of cold pool-induced flow evolution, which significantly alters precipitation evolution in high CAPE simulations. With increased wind speed, precipitation is enhanced in amount and spatial extent. Overall, both low- and high-resolution settings capture the precipitation pattern very similarly in terms of the wind speed, where precipitation becomes observable and the trend in precipitation enhancement, and to a lesser degree the locations of maxima.

Fig. 4 shows the change in the maximum 12h total rainfall with varying wind speeds and domain-integrated rainfall for three different simulation settings. Although there are small discrepancies in very low and some high wind speeds, the degree of agreement is much higher compared to high CAPE simulations. This agreement is also visible in the domain-integrated total rainfall plot. One of the most striking differences between the low and high CAPE simulations is the sensitivity of precipitation to wind speed increments with a much steeper rate. At U40 the system nearly produces double the amount of precipitation (Fig. 3) compared to high CAPE cases (Fig. 4).

In terms of updraft and downdraft intensities (Fig. 5), high resolution 2D and 3D-LES settings show a more invigorated value with the latter setup producing much stronger updrafts. A similar pattern is also apparent in the downdraft plot. When CAPE is lowered to 100 J kg^{-1}, updraft and downdraft intensities are nearly halved compared to 2000 J kg^{-1}. This result indicates that there are other dynamical and physical factors that take place to modulate precipitation distribution and amount, other than updraft intensities or the magnitude of orographic lifting.

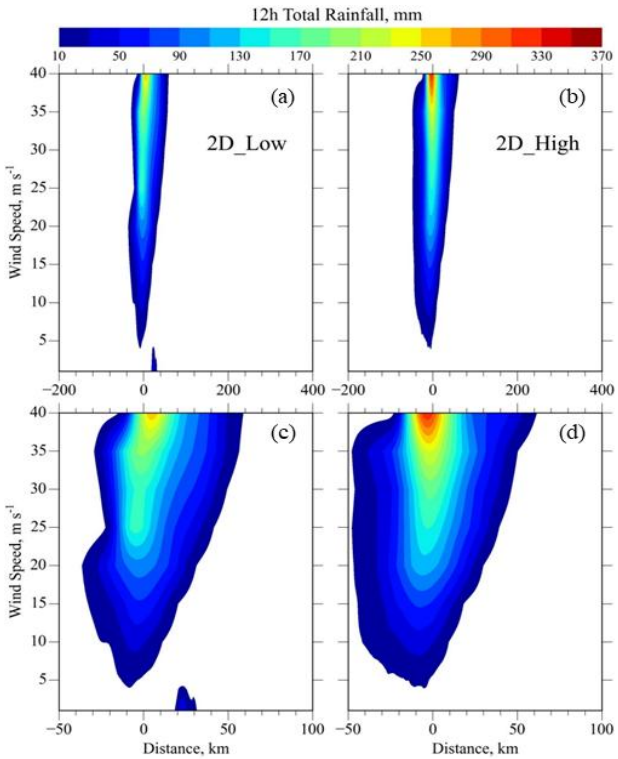

Fig. 3. Distributions and amounts of 12h accumulated rainfall for 2D low-resolution (a and c, Δ*x*=1 km, Δ*z*=0.25 km) and 2D high-resolution (b and d, Δ*x*=0.1 km, Δ*z*=0.1 km) simulations with a low CAPE (100 J kg^{-1}). Panels c and d are the same as a and b, respectively, except for a zoomed-in portion, [-50, 100km], of the total simulation domain [-200, 400 km]

Fig. 6 shows the time evolution of updrafts for U10 and U40 cases for three simulation settings. The differences between 2D-High/3D-LES and 2D-Low are much more pronounced in U40 compared to U10. This might be attributed to intensified microphysics and turbulence interactions that take place in a much denser grid setup at high winds. In both settings, updraft triggering occurs nearly at the same time. There is no distinct updraft triggering signal in the 2D-Low U40 case. At U10, the 2D-High case shows unstable perturbations, yet the other two cases are fairly steady-state throughout the simulation. As the 3D grid allows flow evolution in all three dimensions, updraft values are highest in 3D-LES compared to the other two settings.

Fig. 7 shows the spatial distribution of 12h total precipitation for U10 and U40 cases for three simulation settings. These distributions are significantly different than those in the high CAPE U10 case. At this low wind speed, precipitation is

characterized by stratiform rain, which is concentrated over the upslope of the mountain. Other than the small variations in 2D-Low cases, the results are quite similar for all settings, especially in terms of the right tails of the distributions. As the LFC is lifted higher and the evaporative cooling effect is reduced, precipitation peaks are more than half compared to high CAPE simulations. The total rainfall distributions for U40 2D-High and 3D-LES are almost identical, except for the peaks, which are similar in high CAPE simulations. Apart from the left tail and maximum of total precipitation , 2D-Low shows a similar precipitation pattern. Since the flow is much less turbulent compared to a high CAPE environment, simulation resolution and grid dimensionality have a lesser impact in low CAPE cases.

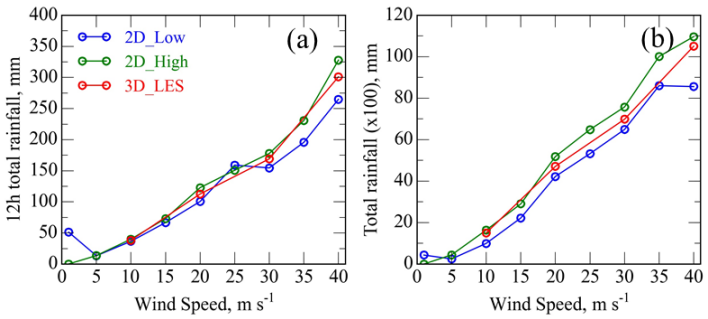

Fig. 4. The 12h total rainfall distributions at 12 h for varying wind speeds (left) and domain-integrated rainfall (right) for low-CAPE (100 J kg^{-1}) simulations with different numerical settings, 2D low- and high-resolution simulations, and 3D LESs

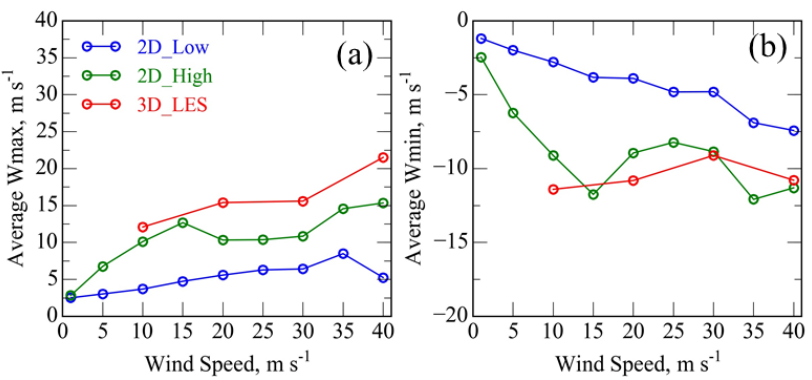

Fig. 5. Domain-averaged (between 2h and 12h) maximum (a) and minimum (b) vertical velocities for varying wind speeds in low-CAPE (100 J kg^{-1}) simulations

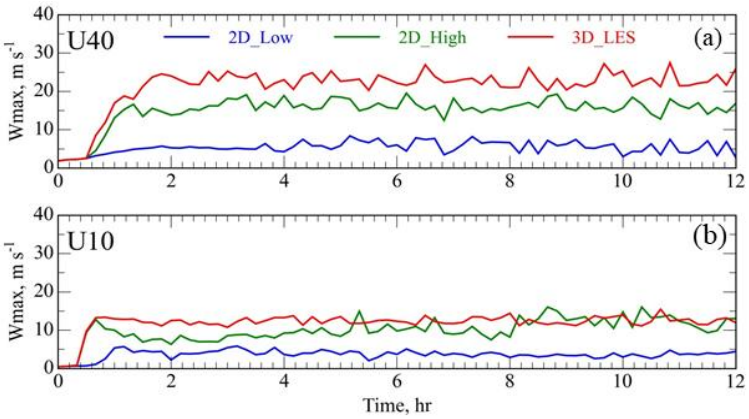

Fig. 6. Time series representation of maximum updraft velocity for (a) U40 and (b) U10 for low-CAPE (100 J kg^{-1}) simulations

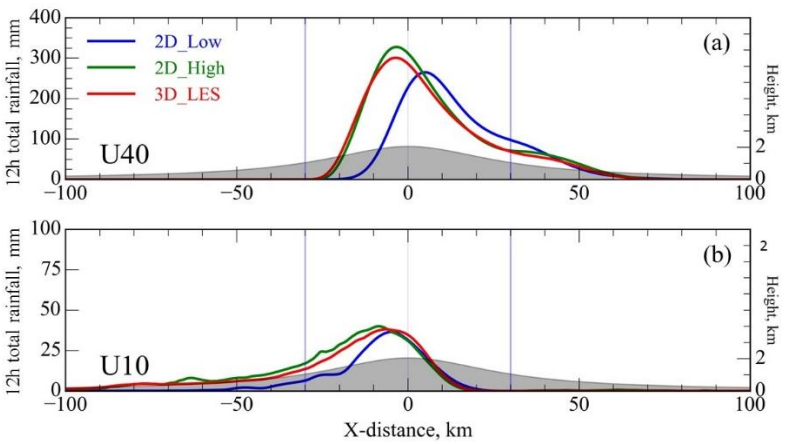

Fig. 7. Total rainfall distributions at 12 h for (a) U40 and (b) U10 over the domain of [-100, 100 km] for low CAPE (100 J kg^{-1}) simulations

4. EVOLUTION OF PRECIPITATING SYSTEM AT HIGHER WINDS

In this section, we study the flow evolution at high wind speeds and highlight some of the differences compared to high CAPE simulations. The results presented in this section are based on 3D-LES simulations.

Hovmöller diagrams of rain rate for three high wind cases are presented in Fig. 8. Going from low to high wind speeds, precipitation shifts rightward due to increased advection and spillover effects. R_{max} is doubled from U20 to U30, yet

not the case for U30 to U40. In the zoomed panels, U20 shows a steady evolution, but U30 and more particularly, U40 show the possible impact of mountain shock on precipitation intensity in the early hours of the simulations. Further on, both simulations continue precipitation in a steady manner. Precipitation maxima are nearly centered on the mountain and do not show much variation among different cases. However, maximum total rainfall (R_{tmax}) varies significantly. From U20 to U30, it is increased from 110 mm to 160 mm, yet at U40 it jumps to 300 mm. This variation highlights the fact that precipitation does not scale linearly with wind speed.

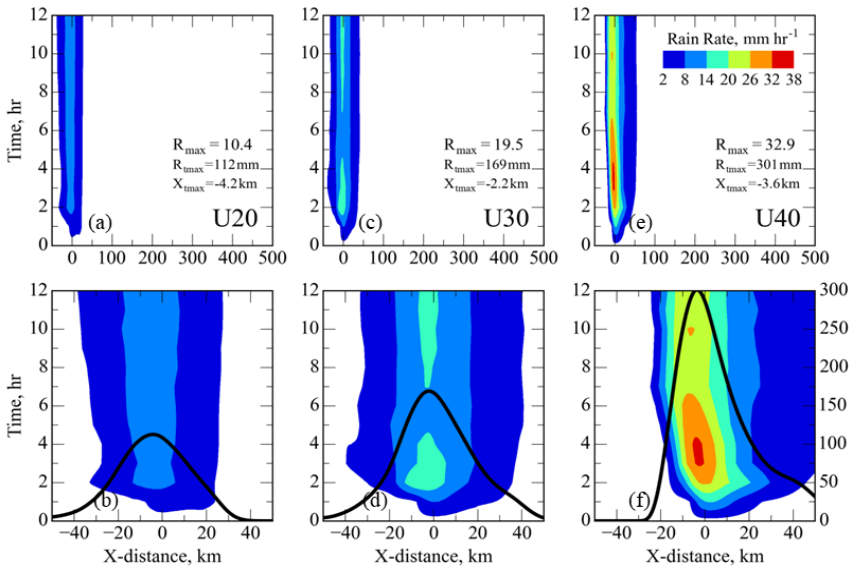

Fig. 8. Hovmöller representation of rainfall rate for U20 (a, b), U30 (c, d) and U40 (e, f) over the domain of [-50, 500 km] (a, c, e) and [-50, 50 km] (b, d, f) for low-CAPE (100 J kg^{-1}) simulations. Basic precipitation statistics, such as maximum rain rate (R_{max}), maximum total rain (R_{tmax}), and the location of maximum total rain (X_{tmax}) are provided in individual panels

Fig. 9 shows the y-average evolution of potential temperature and vertical velocity fields at 3 and 12h. In this case, the cloud envelope is constrained to a narrower margin compared to high CAPE simulations. The depth of cloud increases as the wind speed increases, due to enhanced orographic lifting and more intense updrafts. In the U20 case, an upper-level wave breaking and hydraulic jump signal are present, similar to the U20 case in high CAPE. A wave cloud formation is also visible. Note that as in high CAPE, the wave cloud has nearly no contribution to the precipitation formation. With the increased wind speed, wave-breaking structure vanishes. Updrafts and downdrafts are significantly enhanced and better defined in the U40 case.

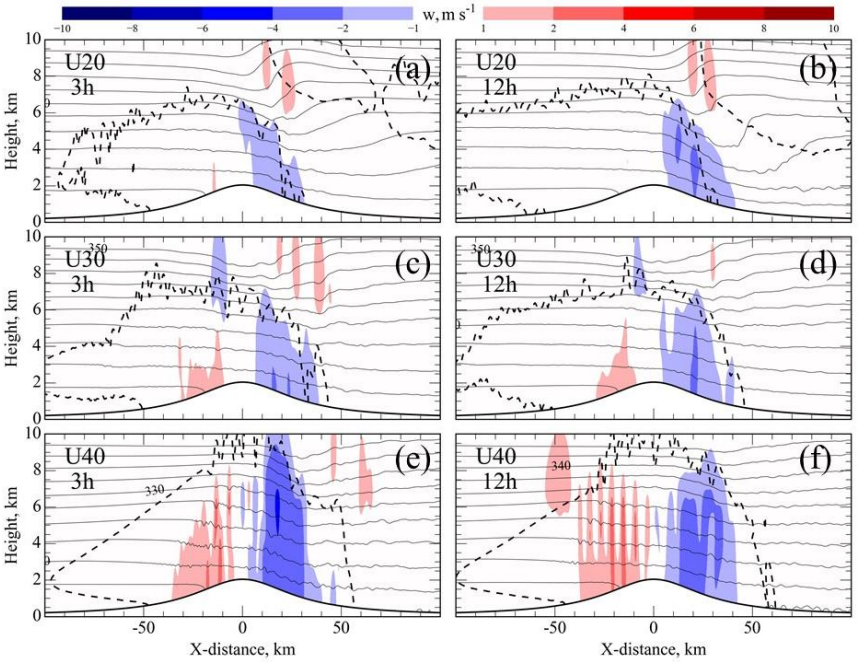

Fig. 9. Evolutions of the along-ridge (y-) averaged potential temperature (thin line contours, plotted at every 5 K), vertical velocity (filled contours in the range of -10 to 10 m s^{-1} with red indicating updraft and blue indicating downdraft regions), cloud envelope (thick dashed line, contoured for the combined hydrometeor values which are greater than 0.1 g kg^{-1}) at 3 h (a, c, e) and 12 h (b, d, f) for U20 (a, b), U30 (c, d) and U40 (e, f) for low CAPE (100 J kg^{-1}) simulations. Plotting domain is zoomed in to 10 km and [-100, 100 km] vertically and horizontally, respectively

In Fig. 10, wind vectors and precipitating hydrometeors are presented for U20, U30 and U40 cases. With increasing wind speed, regions of rain, snow, and graupel are significantly enhanced. The convective cells become much deeper and reach nearly 8 km at U40. In high CAPE cell depth reaches to tropopause and further, as the updrafts are much invigorated in this setup. Wave cloud formation is apparent, yet strong lower-level advection limits the precipitation contribution coming from high levels. There is a slight turbulence signal near the region of wave breaking, which is associated with shear generation, yet this is smaller in magnitude compared to high CAPE simulations (Fig. 11). The majority of the turbulence production is associated with buoyancy production, which is clearly seen from the TKE (gray contours) near the mountain, especially within the region of cloud water production.

The wind vector field reveals that maximum velocities near the surface are enhanced from 39 to 47 m s^{-1} at U20 due to the formation of hydraulic jump.

Once this formation vanishes flow decelerates downslope of the mountain. This flow deceleration can also be attributed to heavy precipitation formation at higher wind speeds. Essentially, some of the incoming kinetic energy will be absorbed in precipitation production and precipitation induced friction slows down the flow.

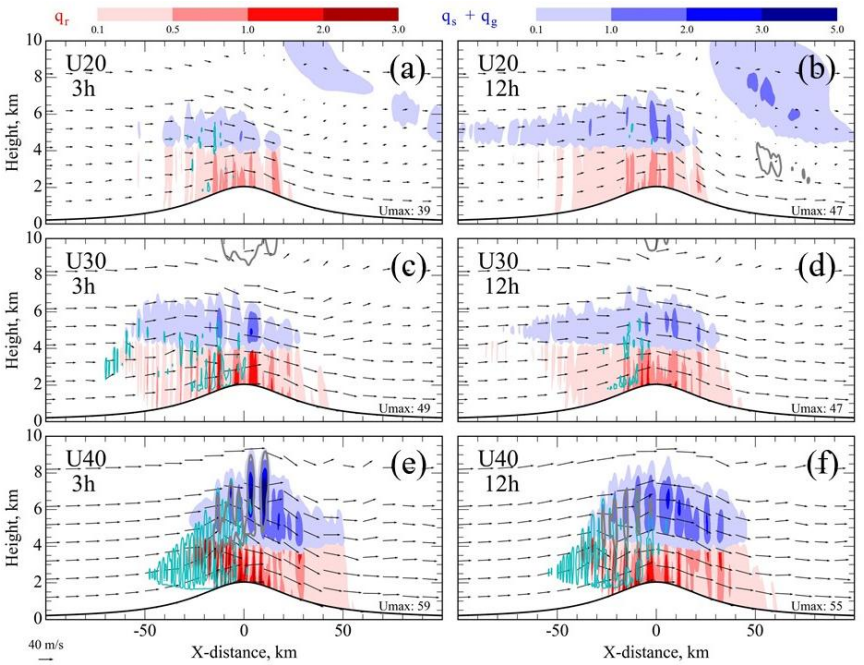

Fig. 10. Evolutions of the along-ridge (y-) averaged warm (q_r: red shadings between 0.1 and 3 g kg^{-1}) and cold (q_s+q_g; blue shadings between 0.1 and 5 g kg^{-1}) hydrometeors and wind vector fields from low CAPE (100 J kg^{-1}) simulations. Cyan line contours show a cloud water mixing ratio that is greater than 1 g kg^{-1} at 3 h (a, c, e) and 12 h (b, d, f) for U20 (a, b), U30 (c, d) and U40 (e, f). Grey line contours show TKE within 1 to 10 m^2 s^{-2} at 5 intervals. Plotting domain is zoomed in to 10 km and [-100, 100 km] vertically and horizontally, respectively. Maximum surface velocities (U_{max} (in m s^{-1}) are included in each panel

Fig. 11 shows an XY view of vertical velocity and TKE at z = 5 km for three wind speeds. When the wind speed increases, the updrafts become more organized. At U40, the flow becomes more two-dimensional and parallel to the 2D mountain ridge; therefore, 3D effects become less important as strong advection in the x-direction does not allow much lateral interaction of large turbulent eddies compared to high CAPE (Fig. 12). Regions of strong downdrafts are not visible in low CAPE cases. At U20, there is a clear TKE signal near the region of wave breaking, yet this signal disappears in other cases. Near the mountain peak, the

buoyancy-induced TKE signal becomes significant as the wind speed and precipitation formation are enhanced.

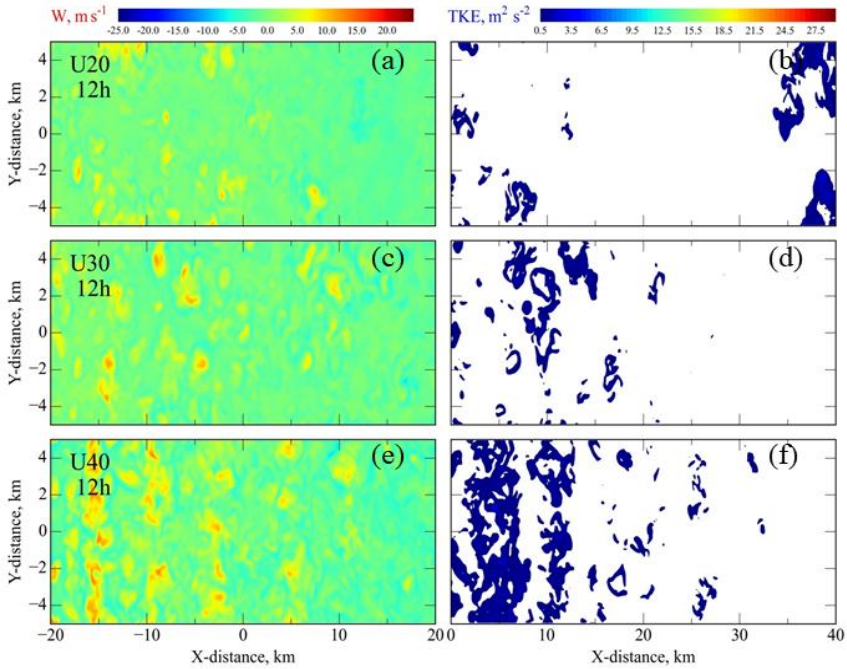

Fig. 11. Simulated 12h vertical velocity fields (a, c, e; in m s^{-1}) in the horizontal domain of [-20, 20 km] x [-5, 5 km] and TKE fields (b, d, f; in m^2 s^{-2}) in the horizontal domain of [0, 40 km] x [-5, 5 km] at *z* = 5 km for U20 (a, b), U30 (c, d) and U40 (e, f) cases. The CAPE is 100 J kg^{-1} for all cases

5. HEAVY PRECIPITATION FORMATION

In order to get a better understanding of heavy precipitation production, the distributions of some of the dynamical and microphysical variables are analyzed in Fig. 12. The top panels show the maximum and minimum vertical velocities for U20, U30 and U40. At U40, updrafts and downdrafts are significantly intensified. This intensification is clearly exhibited in vertically averaged rain, snow and graupel distributions. As in the high CAPE simulations, at high wind speeds, there is no clear correlation between updrafts and regions of hydrometeor peaks as hydrometeors are advected away from their origin. At U20, relatively strong updrafts and downdrafts are a signature of waves breaking downwind of the mountain. Near the surface, the rain mixing ratio is enhanced with increased winds. Compared to high CAPE simulations, this enhancement is much larger.

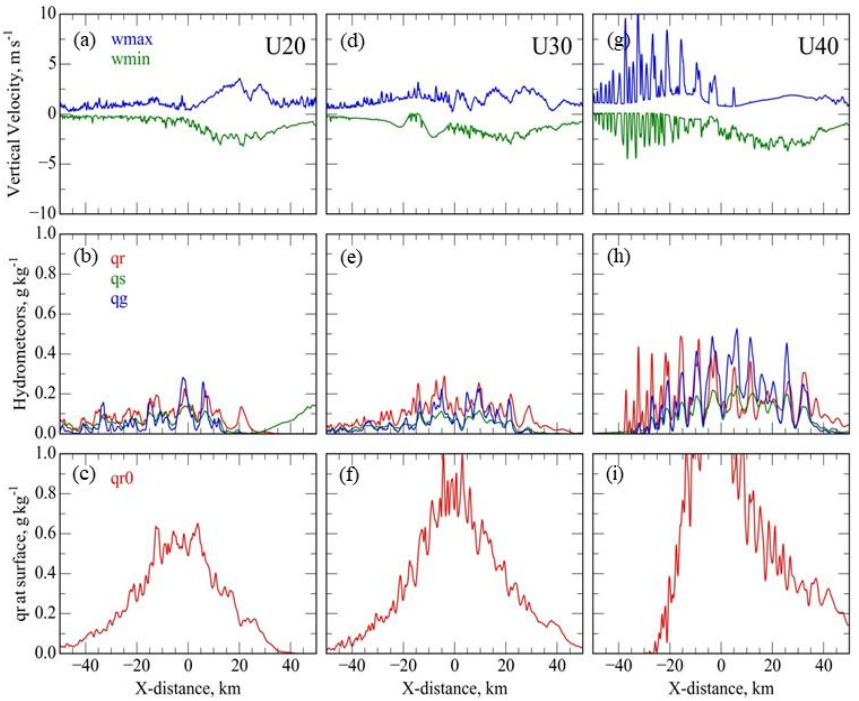

Fig. 12. Maximum and minimum vertical velocities (a, d, g); rain, snow, and graupel mixing ratio distributions (b, e, h) at 12h and fields of rain mixing ratio distribution at surface (c, f, i), which are averaged over the entire simulation for U20 (a, b, c), U30 (d, e, f) and U40 (g, h, i). The CAPE is 100 J kg^{-1} for all cases. The highly varying flow fields can be seen in this zoomed-in horizontal domain of [-50, 50 km]

In order to explain the large precipitation difference between high and low CAPE simulations with high wind speeds, a simple microphysics budget analysis is performed using dominant source and sink terms of rain mixing ratio (q_r) (Figs. 13 and 14). The budget analysis is limited to q_r since the sounding has fairly warm temperatures near the surface. Hence, whichever way precipitation is at higher levels (i.e., ice or mixed phase) only the rain mixing ratio will be scavenged and contribute to the surface precipitation.

The dominant source terms of q_r are: PRACW (accretion of cloud water by rain), PSMLT (melting of snow to rain), PGMLT (melting of graupel to rain), and the dominant sink terms are: PREVP (evaporation of rain). A cumulated summation of these values as well as all other source and sink, and net terms are shown in Figs. 13 (CAPE2000 – high CAPE) and 14 (CAPE100 – low CAPE) over the entire 3D domain. The most dominant source term of the rain mixing ratio is PGMLT for high CAPE and PRACW for low CAPE. This indicates that ice phase

precipitation production is more pronounced in high CAPE, whereas warm rain is a dominant mechanism of rain formation in low CAPE environments. Although the source term is much larger in high CAPE, due to strong evaporation which is associated with strong downdrafts and the fact that the majority of precipitation forms at higher altitudes, the net term is smaller compared to low CAPE. In other words, in low CAPE warm-rain production is more efficient thus rain formed at lower altitudes and has more chance to contribute to the surface rainfall before being advected by strong incoming flow.

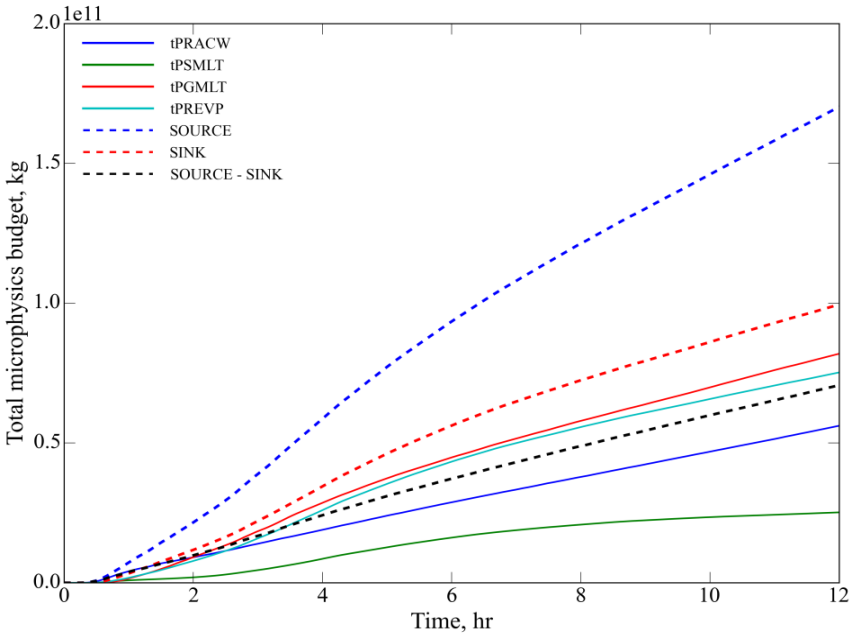

Fig. 13. Simulated dominant budget terms of rain mixing ratio (q_r) for a case with high wind (U = 40 ms^{-1}) and high CAPE (CAPE = 2000 J kg^{-1}) simulation

6. EFFECTS OF MOISTURE, STABILITY, AND WIND SPEED ON OROGRAPHIC FLOW

As the previous section reveals that heavier precipitation is produced at high wind-low CAPE simulations compared to high wind-high CAPE simulations, the role of CAPE is unclear as a control parameter in orographic precipitation studies. For this reason, we designed a series of sensitivity experiments to document the effects of moisture, stability and precipitation on the evolutions of dynamical and physical processes. Based on the flow regime transition argument, which was described in Section 2, the low CAPE simulations which have a more stable atmospheric profile should have yielded upper-level wave breaking at higher wind speeds. Yet wave breaking is observed to cease after

about U = 20 m s^{-1} and the system transitioned to the evanescent regime. This regime transition occurs at about U = 36 m s^{-1} in high CAPE simulations. Since one of the most important differences in low and high CAPE simulations is the precipitation intensities, we intended to investigate the effects of moisture on the flow structure.

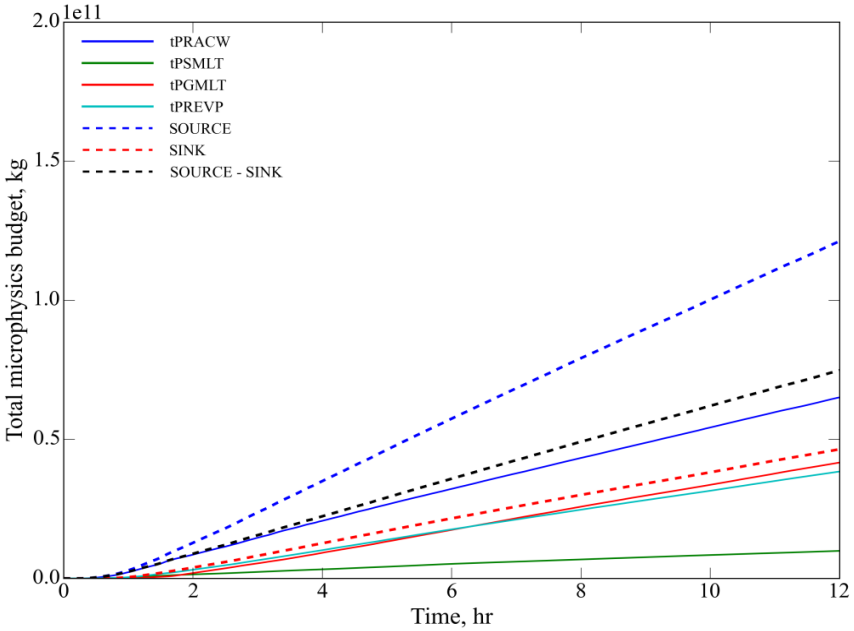

Fig. 14. Simulated dominant budget terms of rain mixing ratio (q_r) for a case with high wind (U = 40 ms^{-1}) and low CAPE (CAPE = 100 J kg^{-1})

Fig. 15 (left panel) shows the set of Brunt-Väisälä frequency profiles (up to model top) used to initialize dry flow simulations. This sounding is constructed with the same CAPE variation method, based on the original sounding. Here, N1 corresponds to a more stable atmosphere, one which has a warmer temperature profile, and N2 is less stable which is representative of a cooler atmosphere. For dry simulations, moisture is set to zero and the microphysics scheme is turned off.

Fig. 15 (right panel) shows the profiles of Brunt-Väisälä frequency that are used to initialize moist flow simulations. Due to moisture effects, the change in stability profiles is visible after the LCL, which is at a similar height for all cases, is reached. Since moisture is considered, this variation is also tied to CAPE when conditional instability occurs. As before, N1 represents the more stable atmosphere with a CAPE of 100 J kg^{-1} and N5 is of a less stable atmosphere with a CAPE of 2000 J kg^{-1}. Here N1 is 0.009, N2 = 0.0085, N3 = 0.0081, N4 =

0.0077, and N5 = 0.0075 s^{-1} which are calculated by averaging the profiles from the surface up to LCL. Using these five profiles and five sets of wind speeds (U01, U10, U20, U30, U40), 25 dry and moist simulations are run based on the same 2D-High setup.

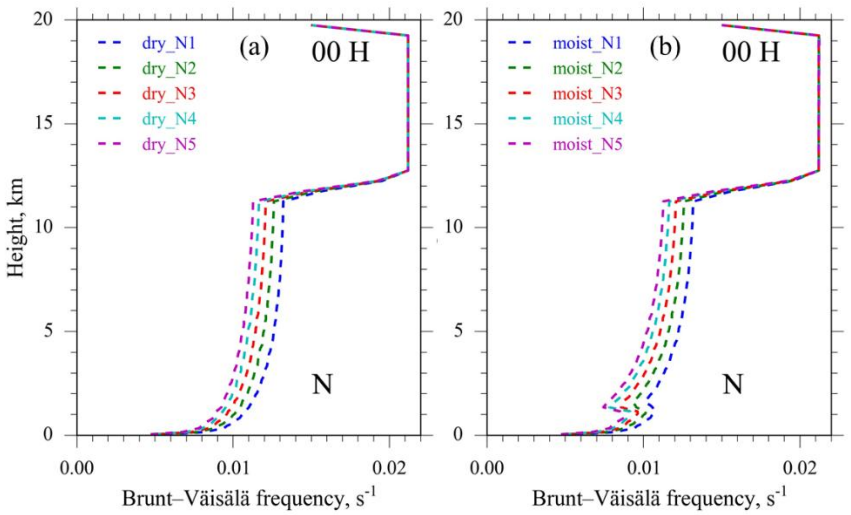

Fig. 15. (a) Dry and (b) unsaturated moist Brunt-Väisälä frequency profiles which are used to initialize sensitivity experiments. Note that N1 to N5 upper-level temperature profiles change from warm to cold. In moist cases, N1, N2, N3, N4, and N5 correspond to (from warmer to colder upper-level profiles) CAPE100, CAPE500, CAPE1000, CAPE1500, and CAPE2000 cases, respectively

At first glance, dry flow simulations (Fig. 16) show a self-similar set of results for each U and N pair, except for cases with higher U and N. This is expected as stability is lower for N4 and N5 cases. From the vertically propagating waves to the evanescent flow transition argument (i.e. Na/U < 2π), the regime transition is expected to occur at lower wind speeds. Simulations that are extended to 50 m s^{-1} (not shown) verify the expectation that dry simulations with higher stability transition to evanescent flow at higher wind speeds. If one were to explain the flow transition based on the Froude number argument (Fr = U/Nh) at U = 30 m s^{-1} (Fr = 2), which is well above the critical Fr =1.12 (Lin 2007) for the system to be in linear regime. Therefore, a second non-dimensional parameter is required, which is the nondimensional mountain width as mentioned above.

For U ≥ 10 m s^{-1}, it is clear that the flow goes over the mountain. For the U10 and U20 sets of simulations, the lower and upper-level wave breaking is apparent, with the lower part causing a hydraulic jump formation. As the vertical wavelength increases with U, the region of lower-level wave breaking is also highlighted. Then at U30, these two features seem to merge. Due to turbulent

mixing extended regions of low- to upper-level turbulent regions are present downwind of the mountain.

The lower-level potential temperature contours of the moist flow simulations do not show a clear signal of flow over mountains (Fig. 17). Though at lower winds the degree of blocking is larger compared to high-wind cases. The moist flow structures of N1/N2, U1-U10-U20 simulations resemble dry cases with a lack of upper-level wave breaking. The flow system in this low CAPE regime is qualitatively analogous to the dry flow regimes studied by Lin and Wang (1996). Then for N4/N5, U20-U30-U40 simulations are similar to dry flow cases with a smoother turbulent signal in moist simulations. This variation in wave perturbations at U40 might be attributed to precipitation effects. For N4/N5, U1-U10 flow structures highly diverge between dry and moist cases. At U1, high CAPE moist cases have a clear blocking signal which is caused by evaporative cooling. This causes an upstream propagation of the precipitating system. Then at U10 localized heavy precipitation alters the flow pattern by limiting the hydraulic jump formation as in the case with dry flow simulations.

The most striking flow structure differences take place for N1-N3, and U30-U40 cases where the CAPE is lower, and precipitation is heavier. In these cases, precipitation formation, both in terms of thermodynamically by latent heat exchanges and mechanically due to drag, severely impacts wave breaking. Hence the dry mountain wave theory cannot be applied directly to these situations even if the moist stability profiles are considered.

A version of the Taylor-Goldstein equation, which includes the effect of viscosity and precipitation, might be helpful to explain the flow evolution in different precipitating scenarios. The linear version of the Taylor-Goldstein equation for a two-dimensional, small-amplitude, inviscid, non-hydrostatic, nonrotating, Boussinesq fluid flow is shown below (Lin, 2007)

$$\left(\frac{\partial}{\partial t}+U\frac{\partial}{\partial x}+\mu\right)^2\left(\frac{\partial^2 w'}{\partial x^2}+\frac{\partial^2 w'}{\partial z^2}\right)+N^2\frac{\partial^2 w'}{\partial x^2}=\frac{\partial^2 \dot{Q}}{\partial x^2} \quad (4)$$

Here $U\frac{\partial}{\partial x}$ represents the advection effect, μ represents the Rayleigh friction and Newtonian cooling, N is the buoyancy, $\frac{\partial^2 \dot{Q}}{\partial x^2}$ term represents the heating effects. In order to represent the highly nonlinear effects that take place in the simulations, precipitation should be accounted for in this equation.

Based on Figs. 16 and 17, the differences between dry and moist, and low and high CAPE simulations may be summarized as: (1) High CAPE cases resemble a more turbulent flow. In this case, moist and dry flow dynamics are more similar in high wind speeds. However, precipitation weakens the magnitude of hydraulic jump; (2) Low CAPE cases resemble a more laminar flow. Moist and dry flow dynamics are more dissimilar in low CAPE and higher wind speeds. Heavy precipitation significantly limits wave breaking and hydraulic wave formation in lower CAPE.

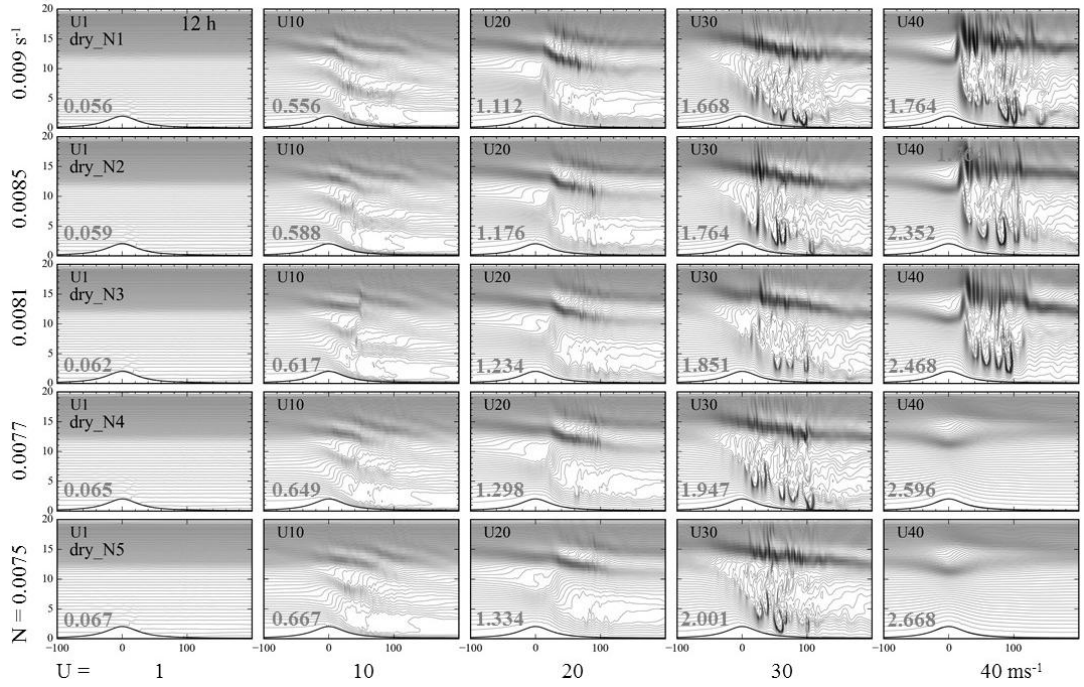

Fig. 16. Potential temperature field for each wind speed (U) and stability (N) case plotted at 2K intervals at 12h for dry flow simulations. The number in gray located in the lower-left corner of each panel is the Froude number (U/Nh)

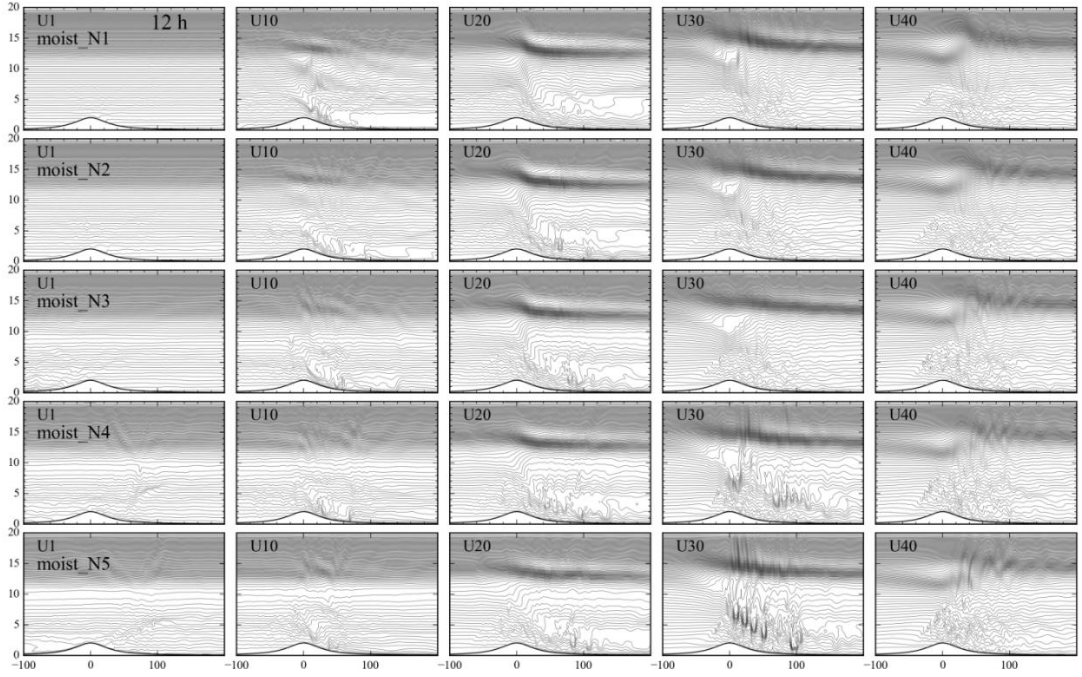

Fig. 17. Potential temperature field for each wind speed (U) and stability (N) case plotted at 2K intervals at 12h for moist flow simulations

7. CONCLUDING REMARKS

Two-dimensional and three-dimensional low- and high-resolution idealized simulations of low CAPE conditionally unstable, uniform basic flow over a bell-shaped mountain have been investigated using the CM1 model. This study extends the findings of previous papers by analyzing the dynamics and physics of flow evolution, precipitation structure and the differences in the flow structure compared to high CAPE simulations.

It was found that the results are less sensitive to dimensionality and resolution in low CAPE simulations as the incoming flow has more laminar characteristics. Particularly at high wind speeds, as the flow is forced to ascend over the mountain, lateral flow interactions are minimal; thus having a third dimension does not have a significant addition to the fidelity of simulations given the high horizontal and vertical resolutions that are employed in the 2D setup.

The precipitating system does not require high CAPE to produce heavy precipitation at high wind speeds. Yet, when CAPE is taken to its lower limit at 100 J kg^{-1}, orographic precipitation at low wind becomes much weaker. In low CAPE, when U is small, the system does not produce any noticeable precipitation, as orographic lifting is not strong enough to trigger convective instabilities by lifting the parcels beyond their LFC. However, when U is pushed over 20 m s^{-1} the system produces steadily heavy precipitation as U increases. In both CAPE simulations, major precipitation is accumulated over at the leeward side of the mountain and distributions get further away from the mountain peak when U is increased. However, opposite to this behavior, the system produces much heavy precipitation at high winds. In fact, the heaviest precipitation is produced when CAPE is low and U is larger, and when CAPE is large, and U is low. Precipitation maximum shifts toward the lee side with increasing CAPE at lower U and cold pool dynamics play an important role. In essence, low CAPE high wind and high CAPE low wind combinations produce the heaviest orographic precipitation.

Dynamical and physical flow evolution analysis which is done based on 3D-LES simulations shows that the system transitions to evanescent flow mode from vertically propagating waves at much earlier wind speeds compared to high CAPE simulations. As the updrafts are weaker in the low CAPE simulations, convective cells are weaker. Yet, contrary to this behavior, more precipitation is formed in low CAPE high wind regimes, as a warm-rain mechanism is more efficient in the warmer sounding. Based on a simple microphysics budget analysis, it was revealed that although a high-CAPE high-wind case has a larger production of ice hydrometeors, large evaporation caused by downdrafts and strong flow advection at higher levels explains the differences between precipitation amounts in high or low CAPE simulations.

Future work should consider simulations with friction and boundary-layer effects, particularly at high wind speeds, as some of the idealized simulations presented in this study might not be a very realistic representation of the atmosphere given

the frictionless boundary conditions. As the ultimate goal of these idealized simulations is to understand flow structure and precipitation formation in a limited environment and apply these findings to real cases, we plan on conducting numerical experiments with soundings representing real TC environments and realistic mountain profiles, as well as real-case simulations of TC and other extreme precipitation cases over a topography.

DISCLAIMER (ARTIFICIAL INTELLIGENCE)

Authors hereby declare that NO generative AI technologies, such as Large Language Models (ChatGPT, COPILOT, etc.) and text-to-image generators, have been used during the writing or editing of this manuscript.

COMPETING INTERESTS

Authors have declared that no competing interests exist.

REFERENCES

Barcilon, A., J. C. Jusem, and P. G. Drazin, 1979: On the two-dimensional, hydrostatic flow of a stream of moist air over a mountain ridge. *Geophys. Astrophys. Fluid Dyn.*, 12, 1–16. doi: 10.1080/03091927908243765

Bryan, G. H., and J. M. Fritsch, 2002: A benchmark simulation for moist nonhydrostatic numerical models. *Mon. Wea. Rev.*, 130, 2917-2928. doi: 10.1175/1520-0493(2002)130<2917:ABSFMN>2.0.CO;2

Chen, S.-H., and Y.-L. Lin, 2005: Effects of moist Froude number and CAPE on a conditionally unstable flow over a mesoscale mountain ridge. *J. Atmos. Sci.*, 62, 331-350. doi: 10.1175/JAS-3380.1

Chen, S.-H., Y.-L. Lin, and Z. Zhao, 2008: Effects of unsaturated moist Froude number and orographic aspect ratio on a conditionally unstable flow over a mesoscale mountain. *J. Meteor. Soc. Japan*, 80, 99-118. doi: 10.2151/jmsj.86.353

Chow, F. K., 2012: *Mountain Weather Research and Forecasting: Recent Progress and Current Challenges.* De Wekker, S. F. J., and B. Snyder (eds)., Berlin: Springer. 750 pp.

Chu, C.-M., and Y.-L. Lin, 2000 (CL00): Effects of orography on the generation and propagation of mesoscale convective systems in a two-dimensional conditionally unstable flow. *J. Atmos. Sci.*, 57, 3817-3837. doi: 10.1175/1520-0469(2001)057<3817:EOOOTG>2.0.CO;2

Colle, B. A., 2004: Sensitivity of orographic precipitation to changing ambient conditions and terrain geometries: An idealized modeling perspective. *J. Atmos. Sci.*, 61, 588-606. doi: 10.1175/1520-0469(2004)061<0588:SOOPTC>2.0.CO;2

Colle, B. A., and Y. Zeng, 2004a: Bulk Microphysical Sensitivities within the MM5 for Orographic Precipitation. Part I: The Sierra 1986 Event. *Mon. Wea. Rev.*, 132, 2780-2801. doi: 10.1175/MWR2821.1

Houze, R. A., Jr., 2012: Orographic effects on precipitating clouds. *Rev. Geophys.*, 50, RG1001, doi:10.1029/2011RG000365

Huang, Y.-C., and Y.-L. Lin, 2014: A study on the structure and precipitation of Morakot (2009) induced by the Central Mountain Range of Taiwan. *Meteor. Atmos. Phys.*, 123, 115-141. doi: 10.1007/s00703-013-0290-4.

Lin, Y.-L., 2007: *Mesoscale Dynamics*. Cambridge University Press, 630 pp.

Lin, Y.-L., and T.-A. Wang, 1996: Flow regimes and transient dynamics of two-dimensional stratified flow over an isolated mountain ridge. *J. Atmos. Sci.*, 53, 139-158. doi: 10.1175/1520-0469(1996)053<0139:FRATDO>2.0.CO;2

Lin, Y.-L., S. Chiao, T.-A. Wang, and M. L. Kaplan, 2001: Some common ingredients for heavy orographic rainfall. *Wea. Forecasting*, 16, 633-660. doi: 10.1175/1520-0434(2001)016<0633:SCIFHO>2.0.CO;2

Lin, Y.-L., R. D. Farley, and H. D. Orville, 1983: Bulk parameterization of the snow field in a cloud model. *J. Appl. Meteor.*, 22, 1065–1092. doi: 10.1175/15200450(1983)022<1065:BPOTSF>2.0.CO;2

Miglietta, M. M., and R. Rotunno, 2009 (MR09): Numerical simulations of conditionally unstable flows over a mountain ridge. *J. Atmos. Sci.*, 66, 1865–1885. doi: 10.1175/2009JAS2902.1

Miglietta, M. M., and R. Rotunno, 2010: Numerical simulations of low-CAPE flows over a mountain ridge. *J. Atmos. Sci.*, 67, 2391–2401. doi: 10.1175/2010JAS3378.1

Miglietta, M. M., and R. Rotunno, 2014: Numerical simulations of sheared conditionally unstable flows over a mountain ridge. *J. Atmos. Sci.*, 71, 1747–1762. doi: 10.1175/JAS-D-13-0297.1

Nugent, A. D., R. B. Smith, and J. R. Minder, 2014: Wind speed control of tropical orographic convection. *J. Atmos. Sci.*, 71, 2695-2712. doi:10.1175/JAS-D-13-0399.1

Raymond, D. J. and R. Rotunno, 1989: Response of a stably stratified flow to cooling. *J. Atmos. Sci.*, 46, 2830–37. doi: 10.1175/1520-0469(1989)046<2830:ROASSF>2.0.CO;2

Rostom, R., and Y.-L. Lin, 2021: Common Ingredients and Orographic Rain Index (ORI) for Heavy Precipitation Associated with Tropical Cyclones Passing over the Appalachian Mountains. Earth Sci. Research, Vol. 10, No. 1. doi:10.5539/esr.v10n1p32.

Sawyer, J. S., 1956. The physical and dynamical problems of orographic rain. Weather, 11, 375–381.

Schalkwijk, J., H. J. J. Jonker, A. P. Siebesma, and E. Van Meijgaard, 2015: Weather forecasting using GPU-based large-eddy simulations. *Bull. Amer. Meteor. Soc.*, 96, 715-723. doi: 10.1175/BAMS-D-14-00114.1

Schlesinger, R. E., 1978: A three-dimensional numerical model of an isolated thunderstorm: Part I. Comparative experiments for variable ambient wind shear. *J. Atmos. Sci.*, 35, 690–713.

Sever G, and Y.-L. Lin, 2017: Dynamical and physical processes associated with orographic precipitation in a conditionally unstable uniform flow: Variation in basic wind speed. *J. Atmos. Sci.*, 74, 449-66. doi: https://doi.org/10.1175/JAS-D-16-0077.1

Smith, R. B., 1979: The influence of mountains on the atmosphere. Adv. in Geophys., 21, 87–230. doi: 10.1016/S0065-2687(08)60262-9

Smith, R.B., P. Schafer, D. Kirshbaum, and E. Regina, 2009: Orographic Enhancement of Precipitation inside Hurricane Dean. *J. Hydrometeor.*, 10, 820–831. doi:10.1175/2008JHM1057.1

Tao, W.-K., and J. Simpson, 1993: Goddard Cumulus Ensemble Model. Part I: Model description. *Terr. Atmos. Ocean. Sci.*, 4, 35-72.

Wang, T.-A., and Y.-L. Lin, 1999: Wave ducting in a stratified shear flow over a two-dimensional mountain. Part II: Implications for the development of high-drag states for severe downslope windstorms. *J. Atmos. Sci.*, 56, 437-452. doi: 10.1175/1520-0469(1999)056<0437:WDIASS>2.0.CO;2

Weisman, M. L., and J. B. Klemp, 1982: The dependence of numerically simulated convective storms on vertical wind shear and buoyancy. *Mon. Wea. Rev.*, 110, 504–520. doi: 10.1175/1520-0493(1982)110<0504:TDONSC>2.0.CO;2

Witcraft, N. C., Y.-L. Lin, and Y.-H. Kuo, 2005: Dynamics of orographic rain associated with the passage of a tropical cyclone over a mesoscale mountain*. Terr. Atmos. Ocean*, 16, 1133-1161.

Xue, M., K. K. Droegemeier, and V. Wong, 2000: The Advanced Regional Prediction System (ARPS) - A multiscale nonhydrostatic atmospheric simulation and prediction tool. Part I: Model dynamics and verification. *Meteor. Atmos. Physics.*, 75, 161-193. doi: 10.1007/s007030070003

Yang, M.-J., S. A. Braun, and D.-S. Chen, 2011: Water budget of Typhoon Nari (2001). *Mon. Wea. Rev.*, 139, 3809–3828, doi: 10.1175/MWR-D-10-05090.1.

Biography of author(s)

Yuh-Lang Lin
North Carolina A&T State University, Greensboro, North Carolina, USA.

He is a professor at the Physics Department and Applied Science and Technology Ph.D. Program, North Carolina A&T State University. He teaches courses covering atmospheric dynamics and modeling. He has published more than 140 articles on Mountain Meteorology, Moist Convection, Wildfire Dynamics, Numerical Weather Prediction, Tropical Cyclone Dynamics, and Cloud Microphysics Parameterizations (with 9627 citations on Google Scholar & listed as World's top 2% scientists by Stanford U. in 2020).

Peer-Review History:
This chapter was reviewed by following the Advanced Open Peer Review policy. This chapter was thoroughly checked to prevent plagiarism. As per editorial policy, a minimum of two peer-reviewers reviewed the manuscript. After review and revision of the manuscript, the Book Editor approved the manuscript for final publication. Peer review comments, comments of the editor(s), etc. are available here: https://peerreviewarchive.com/review-history/4126